Strong quantum interferences in frequency up-conversion towards short vacuum-ultraviolet radiation pulses

Patric Ackermann,* Alexander Scharf, and Thomas Halfmann
Technische Universität Darmstadt, Institut für Angewandte Physik, Hochschulstraße 6, 64289 Darmstadt
(Received 17 March 2014; published 10 June 2014)

We present experimental data on quantum interferences in resonantly enhanced frequency up-conversion towards the vacuum-ultraviolet spectral regime. The process is driven in xenon atoms by ultrashort (picosecond) laser pulses. We use two simultaneous frequency conversion pathways via an excited intermediate state, i.e., fifth harmonic generation of the fundamental wavelength and four-wave mixing of the fundamental and two photons of its second harmonic wavelength. Both conversion pathways yield radiation at 102 nm. The two pathways interfere, depending on the relative phase of the fundamental and second harmonic. By appropriate choice of the phase we get constructive interference (resulting in increased conversion efficiency) or destructive interference (resulting in reduced conversion efficiency). The total conversion yield shows very pronounced constructive and destructive quantum interference with a visibility of roughly 90%. A stable and highly accurate phase control setup enables such strong quantum interferences for more than 260 oscillation cycles. In an extension of the experiment, simultaneously to frequency conversion we also monitor laser-induced fluorescence as a measure for the excitation probability to the excited intermediate state. Also, in the excitation probability we observe strong quantum interferences. As an interesting feature, a small phase lag occurs between the quantum interference patterns of frequency conversion and population transfer. This is due to an additional atomic phase acquired during frequency conversion.

DOI: 10.1103/PhysRevA.89.063804 PACS number(s): 42.65.Ky, 32.80.Qk, 42.50.Gy

I. INTRODUCTION

The coherent nature of laser radiation enables the investigation of many stunning phenomena, based not only on the high intensity of the driving laser fields, but also the coherence of the interaction. One prominent effect are quantum interferences in atomic or molecular systems. Variation of the relative phase of two indistinguishable excitation pathways (i.e., transitions, simultaneously driven by multicolor laser fields) enables constructive or destructive interference for the total excitation probability. The relative phase of the driving multicolor laser fields serves as a control parameter to suppress or enhance the excitation probability.

The basic concept of such coherent control or "phase control" was introduced by Brumer and Shapiro [1,2], and since then there have been numerous demonstrations in physics and chemistry. However, the vast majority of such experiments aimed at control of branching ratios in chemical reactions or photofragmentation processes, e.g., photodissociation or photoionization. In particular, there are only very few phase control experiments in nonlinear optics [3–6], though this exhibits a highly active field in laser-based physics, e.g., serving to extend the application range of lasers by frequency conversion processes to new wavelength regimes. Important aims in this context are, e.g., generation of long infrared wavelengths or very short wavelengths in the regime of VUV or XUV radiation by nonlinear frequency conversion processes. Such processes are typically driven by high-intensity, ultrafast laser pulses. Nevertheless, the obtained frequency conversion yields are usually very low. Tuning the lasers to atomic (multiphoton) resonances exhibits a way to increase the conversion efficiencies. Quantum interferences permit control (i.e., suppression or enhancement) of such resonant frequency conversion processes.

Quantum interferences in frequency conversion rely on the interference of two indistinguishable frequency conversion pathways. A typical example is, e.g., two different frequency mixing processes yielding the same output frequency. A constant and controllable phase relation between the driving radiation fields is required to drive constructive and destructive interference (depending on the phase). In our experiments, we implemented a phase control scheme for resonantly enhanced frequency up-conversion of picosecond radiation pulses towards the VUV regime. In contrast to the few previous works on phase control in nonlinear optics, we apply ultrashort (picosecond) laser pulses and aim at strong control of high-order frequency conversion processes towards short VUV wavelengths.

We observe very strong quantum interferences with a visibility of more than 90%. To our knowledge, this value exhibits the highest control achieved in frequency up-conversion by quantum interferences (and a very large value also compared to arbitrary phase control experiments) to date. As we will discuss below, we achieved the large visibility by carefully matching conversion strengths, also taking averaging effects in the interaction volume into account, as well as proper measurement and control of relative laser phases by a specific setup. The demonstration of high visibility at short pulse durations (and extended bandwidth) is of interest for applications in ultrafast nonlinear optics, e.g., high-harmonic generation.

In parallel to phase control of frequency conversion, we also investigate quantum interferences in the excited-state population by simultaneously acquiring laser-induced fluorescence. As an interesting feature, we observe a consistent phase lag between the quantum interference traces of frequency conversion and fluorescence (i.e., excited-state population). We attribute this phase lag to atomic phases in the excitation process.

*patric.ackermann@physik.tu-darmstadt.de

II. COUPLING SCHEME

In our experiment we investigate quantum interference in frequency up-conversion in a dense supersonic jet of xenon atoms. Xenon exhibits large susceptibilities for frequency conversion towards the VUV and XUV spectral regime. We drive two indistinguishable frequency conversion processes: Fifth harmonic generation of fundamental radiation at a wavelength of $\lambda_F = 512$ nm, as well as simultaneous four-wave mixing of two photons of the second harmonic ($\lambda_{SHG} = 256$ nm), and one photon of the fundamental radiation field (see Fig. 1). The transition between the ground state $5p^6\,{}^1S_0$ and the excited state $6p\,{}^2[5/2]_2$ is resonant for four photons of the fundamental or two photons of the second harmonic driving field. One additional fundamental photon couples the excited state $6p\,{}^2[5/2]_2$ to the dense manifold of Rydberg states ($n = 26$–28). The conversion processes yield signal radiation at $\lambda_S = 102.4$ nm.

In case of resonant excitation, some population is transferred to state $6p\,{}^2[5/2]_2$. Since the lifetime of this level (35 ns [7]) is much longer than the interaction time, the population dynamics are dominated by coherent optical excitation. After the interaction the atoms decay to the excited state $6s^2[3/2]_0$, yielding laser-induced fluorescence (LIF) at a wavelength of 992.3 nm [8].

In the quantum interference experiment, we investigate the conversion yield towards radiation at $\lambda_S = 102.4$ nm vs the phase difference between the two driving laser pulses. Driven by the fundamental field $\mathcal{E}_F(r,z,t) = E_F(r,z)e^{i(\omega_1 t+\varphi_1)} + \text{c.c.}$, with the electric field amplitudes $E_F = E_F(r,z)$, we get the nonlinear polarization for fifth harmonic generation

$$P^{(5)}_{5HG} \propto \chi^{(5)}_{5HG}\left(E_F^5 e^{-i(5\omega_F)t}e^{-i5\varphi_F} + \text{c.c.}\right), \tag{1}$$

involving the phase φ_F of the fundamental pulse. The nonlinear polarization of the four-wave mixing process involves the second harmonic field $\mathcal{E}_{SH}(r,z,t) = E_{SH}(r,z)e^{i(\omega_{SH}t+\varphi_{SH})} + \text{c.c.}$. We choose the absolute phase of the second harmonic as reference, i.e., $\varphi_{SH} = 0$, and write the polarization for the four-wave mixing process,

$$P^{(3)}_{FWM} \propto \chi^{(3)}_{FWM}\left(E_{SH}^2 e^{-i(2\omega_{SH})t}E_F e^{-i(\omega_F)t}e^{-i\varphi_F} + \text{c.c.}\right). \tag{2}$$

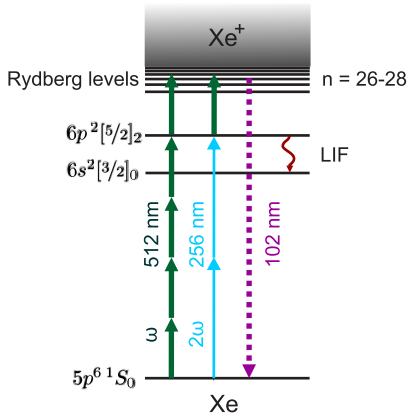

FIG. 1. (Color online) Coupling scheme with relevant energy levels and transitions.

In the following, we assume an optically thin medium, permitting almost perfect phase matching and negligible pump depletion. We confirmed that this assumption is well justified in our setup. The real part of the cycle-averaged intensity at $5\omega_F$ can be estimated,

$$Re\{I_{VUV}\} \propto \int_L |\tilde{P}^{(3)}_{FWM}|2 + |\tilde{P}^{(5)}_{5HG}|2 + 2\text{Re}\left[\tilde{P}^{(5)}_{5HG}\tilde{P}^{(3)}_{FWM}\right]\cos(4\varphi_F + \Delta_\chi)\,dz, \tag{3}$$

with the (complex) polarization amplitudes $\tilde{P}^{(3)}_{FWM} = \chi^{(3)}_{FWM}E_1E_2^2$ and $\tilde{P}^{(5)}_{5HG} = \chi^{(5)}_{5HG}E_1^5$ and the length of the medium L. Here Δ_χ is the phase difference of both induced polarizations at $\varphi_F = 0$. This phase difference results from the phase of the electronic dipole moments involved in each nonlinear susceptibility. We note that the nonlinear susceptibilities $\chi^{(3)}_{FWM}$ and $\chi^{(5)}_{5HG}$ involve contributions of transitions from the state $6p\,{}^2[5/2]_2$ to all Rydberg levels. To maximize the interferometric visibility, we must match the polarization amplitudes of four-wave mixing and fifth harmonic generation, e.g., by adjusting the second harmonic intensity.

The generated intensity oscillates four times during a phase shift of 2π of the fundamental radiation field. The phase difference Δ_χ could only be determined by knowledge of the absolute phase difference $\varphi_F - \varphi_{SH}$ of the driving laser fields. In our experiment, we can measure variations in φ_F only. Thus we cannot deduce the absolute phase, which is no problem anyway, as we are interested in the quantum interference oscillations and period only.

We also investigate the fluorescence yield from the excited state $6p\,{}^2[5/2]_2$. In contrast to the frequency mixing signal, the probability W to populate the excited state involves the two dipole moments for two-photon ($\mu^{(2)}$) and four-photon ($\mu^{(4)}$) transition only [9]:

$$W \propto \left[\mu^{(4)}E_F^4\right]^2 + \left[\mu^{(2)}E_{SH}^2\right]^2 + 2\mu^{(4)}\mu^{(2)}E_F^4E_{SH}^2\cos(4\varphi_F + \Delta_\mu). \tag{4}$$

Consequently, the phase difference of the two dipole moments Δ_μ shows up as a phase shift of the interference pattern for $\varphi_F = 0$.

Thus, comparison of the quantum interferences for frequency conversion and the population of the excited state (i.e., measured by fluorescence) can reveal the difference $\Delta_\chi - \Delta_\mu$ in atomic phase contributions.

III. EXPERIMENTAL SETUP

The experimental setup (see Fig. 2) is as follows: A titanium sapphire oscillator (MIRA 900P, Coherent), pumped by a frequency-doubled, continuous-wave Nd:YVO laser (VERDI V18, Coherent), generates laser pulses with a pulse duration of 1.8 ps (FWHM) at a wavelength of 800 nm. The pulse train synchronously pumps an optical parametric oscillator (OPO) with intracavity frequency doubling (OPO FAN, APE). The oscillator provides tunable (picosecond) radiation pulses in the visible regime with linear polarization. The pulse energy is around 2 nJ at a repetition rate of 76 MHz and a pulse length of 0.9 ps (FWHM). For our experiment we operate the OPO with tunable output wavelengths in the range of 512–514 nm.

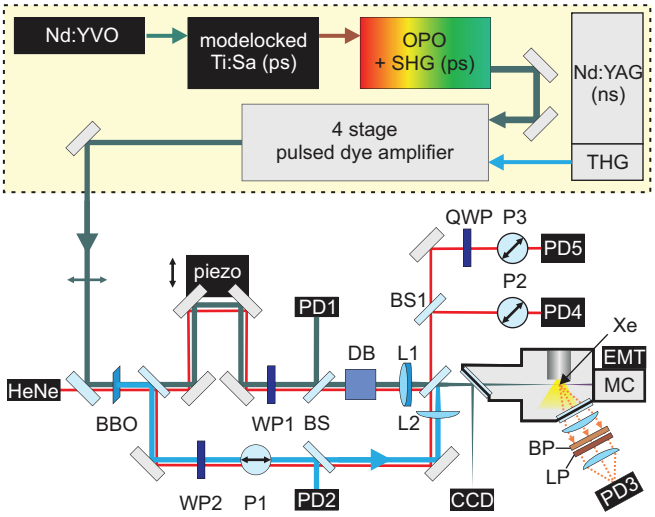

FIG. 2. (Color online) Experimental setup. (WP: half wave plates, QWP: quarter wave plate, BS: beam sampler, DB: dispersion block, L: lenses, P: polarizers, PD: photodiodes, BP: bandpass filter, LP: longpass filter, MC: vacuum monochromator, Xe: jet of xenon atoms).

The picosecond pulses from the OPO are amplified in a homemade four-stage dye amplifier chain. We use Coumarine 540A in a solution of 91% 1-4-dioxane and 9% ethylene glycol in the first two dye cells and Coumarine 504 solved in methanol in the third and fourth dye cell. The third harmonic of a nanosecond pulsed, injection-seeded Nd:YAG laser (Pro 230-20, QuantaRay) with typical pulse energies of 350 mJ (third harmonic) serves to pump the dye amplifier chain. After each of the four amplification stages, we spatially filter the amplified pulses. We obtain typical amplified pulse energies of up to 200 μJ at a pulse duration of 1.15 ps, a bandwidth of 0.80 nm, and some residual group delay dispersion of 1.1 ps THz^{-1}. The amplified pulses are frequency doubled in a β-barium-borate (BBO) crystal (length 500 μm), yielding a typical pulse energy of 20 μJ in the second harmonic around 256 nm.

In this setup, the phases of the two laser beams are automatically phase locked to each other. We note that in principle phase distortions can occur during frequency doubling, if parametric backconversion is not negligible or the nonlinear refractive index is large. We avoid such effects by using a thin (500 μm) BBO crystal.

The fundamental and second harmonic pulses enter a Mach-Zehnder interferometer-type setup to vary pulse delays, i.e., the relative phases between the pulses (see lower part of Fig. 2). The second harmonic propagates along one arm of the setup with fixed path length. A variable attenuator, consisting of a zero-order half wave plate (WP2) and a polarizer (P1), permits one to modify the intensity of the second harmonic, i.e., to match the strength of the two frequency conversion pathways in the quantum interference experiment. The fundamental wavelength propagates along the second arm of the setup, which contains a variable delay line with a piezoactuator. An achromatic half wave plate serves to align the polarization of the fundamental radiation parallel to the second harmonic. A dispersion block (DB, H-ZLAF52 glass, length 35.6 mm) compensates for group delay dispersion of 0.038 ps THz^{-1}, generated by dispersion for the second harmonic in the optical elements of the Mach-Zehnder setup. The dispersion would otherwise lead to wavelength-dependent delays of the fundamental and second harmonic pulses. The dispersion block enables us to keep the time delay of the two beams constant over a wavelength range of 10 nm. We focus both radiation beams into a jet of xenon atoms, expanded through a pulsed nozzle (General Valve, stagnation pressure 1 bar, orifice diameter 0.8 mm) in a vacuum chamber. The interaction region with the laser beams is right behind the nozzle opening, i.e., less than 1 mm downstream the atomic jet, resulting in an estimated gas density of about 10^{17} cm^{-3} [10].

We use a $f = 250$ mm achromatic lens (L1) to generate a focal spot of 48 μm (FWHM) for the fundamental and a $f = 300$ mm fused silica lens (L2) to generate a focal spot of 36 μm (FWHM) for the second harmonic in the interaction region. The Rayleigh length of the two focal volumes are 11 mm for the fundamental beam and 12 mm for the second harmonic beam. As the Rayleigh lengths are large compared to the diameter of the atomic jet, effects of the Gouy phase play no role. Furthermore, we neglect phase-matching effects, as we estimate the maximal possible phase mismatch to be below $\pi/4$. We note that large contrast in quantum interferences requires that for each position in the interaction volume the two interfering pathways (in our case, the two frequency conversion processes) are equally strong. Thus spatial averaging over laser intensity distributions can completely wash out quantum interferences. When the intensities inside the interaction region satisfy the condition

$$I_F^4 / I_{SH}^2 = const. \tag{5}$$

along the transversal direction, there are no effects of spatial averaging. Thus the optimal ratio of focal spot diameters in our experiment would be $d_F/d_{SH} = \sqrt{2}$. We note that for this value condition (5) is automatically fulfilled along the whole laser beam path. This is consistent with numerical simulations of our frequency conversion process inside the interaction region (as also shown in [11] for two-photon vs one-photon quantum interferences). Our actual spot size ratio of 4/3 is very close to the optimal value of $\sqrt{2}$.

We finally match the nonlinear polarizations of four-wave mixing and fifth harmonic generation by strong attenuation of the second harmonic beam with a zero-order half wave plate and an α-BBO polarizer. Typical pulse energies for optimal visibility are 110 μJ for the fundamental and 0.5 μJ for the second harmonic beam.

A monochromator (MC) separates the generated VUV radiation from the fundamental and second harmonic beam and directs it onto an electron multiplier (EMT R595, Hamamatsu) for detection. The signal from the EMT passes an amplifier (FEMTO DHPVA-100) and a boxcar gated integrator (SR250, SRS).

Parallel to the experiment, we monitor the pulse energies of fundamental and second harmonic beam on photodetectors (PD1 & PD2, Becker&Hickl PDI400), as well intensity distribution and spatial overlap in the focal spots on a

CCD sensor (The Imaging Source DMM 315403ML) with a removed cover glass.

In addition to frequency conversion, we also record laser-induced fluorescence from the excited intermediate state. The fluorescence at 992.3 nm [8] is collimated by a lens system with focal length $f = 75$ mm orthogonal to the laser beam and the xenon jet. The radiation propagates through a bandpass filter (BP, center wavelength 990 nm), a long pass filter (cutoff wavelength 950 nm), and is focused onto a photodiode for detection. The signal is amplified by a current amplifier (FEMTO DLPCA-200) before further data processing.

We now briefly discuss an important technical extension of the setup, which serves to precisely measure the relative phase between the two driving radiation fields, i.e., the difference between the path lengths in the Mach-Zehnder interferometer-type setup. Precise determination (and hence controlled variation) of the phase is crucial for pronounced quantum interferences, i.e., large contrast. To determine the phase difference, we use a helium-neon (HeNe) reference laser (Melles-Girot 05-LRH/P-151, wavelength stability $<$ 0.004 nm), collinearly coupled into the Mach-Zehnder setup.

Thus the delay line for the fundamental and second harmonic beam is used as a Mach-Zehnder interferometer for the HeNe laser. The initial polarization of the HeNe laser is linear and vertical. The achromatic half wave plate in the upper arm of the interferometer rotates the polarization of the HeNe laser to horizontal. The zero-order half wave plate (256 nm) in the lower arm of the interferometer has negligible effect on the polarization of the HeNe laser. Thus we end up with two collinear laser beams with orthogonal polarizations at the exit of the interferometer (in front of BS1). Behind the interferometer, we project the polarizations onto a common polarization axis by a polarizer (P2), which is tilted by 45 degrees, to get a interference signal at a photodiode (PD4). Analysis of the interference signal vs voltage on the piezo actuator in the delay line already provides information on the relative path length difference in the interferometer. However, we require a second interference signal to eliminate otherwise ambiguous information at the minima and maxima of the first interference trace. This second signal is generated by inserting an achromatic quarter wave plate (QWP) before the polarizer P3, such that the vertical polarized beam is retarded by a quarter wavelength with respect to the horizontal polarized beam. We project both polarizations onto a polarization axis under 45° and detect the signal by a photodiode (PD5). This resolves ambiguous information at specific phase values in the first interference trace. Processing both interference signals, we obtain the path difference in the Mach-Zehnder setup with an accuracy better than 5 nm, corresponding to a phase accuracy of $\Delta\varphi_F = 10^{-2} \times 2\pi$.

We note that precise determination of the phase difference also enables stable phase variations in a large interval. Thus our setup permits interferometrically stable and continuously controlled phase variations corresponding to pulse delays of more than 110 fs. As we will show below, this precision and stability of our phase control setup serves to monitor pronounced quantum interferences for a very large number of oscillation cycles.

IV. RESULTS

In a first experiment we monitor the variation of the frequency conversion processes vs the phase difference of the fundamental and second harmonic laser pulses. We tune the fundamental wavelength exactly to the (theoretically known [8]) four-photon resonance at $\lambda_F = 512$ nm [see Fig. 3(a)].

As the VUV intensity depends in higher order upon the laser intensity, we monitor the fundamental laser intensity in parallel to VUV acquisition and record only data points in a small window of $\pm 7\%$ around the central fundamental intensity. The VUV intensity vs phase difference shows a very strong modulation, yielding large visibility

$$v = \frac{I_{\max} - I_{\min}}{(I_{\max} + I_{\min})}$$

of 76% as deduced from a sine fit.

We slightly detune the fundamental laser frequency now to the red side of the resonance at $\lambda_F = 512.7$ nm. Hence the second harmonic frequency is now $\lambda_{SHG} = 256.3$ nm. As a surprising feature, the visibility for detuned excitation even becomes larger and now reaches 90% [see Fig. 3(b)]. We attribute this to dynamic Stark shifts of the $6p^2[5/2]_2$ resonance,

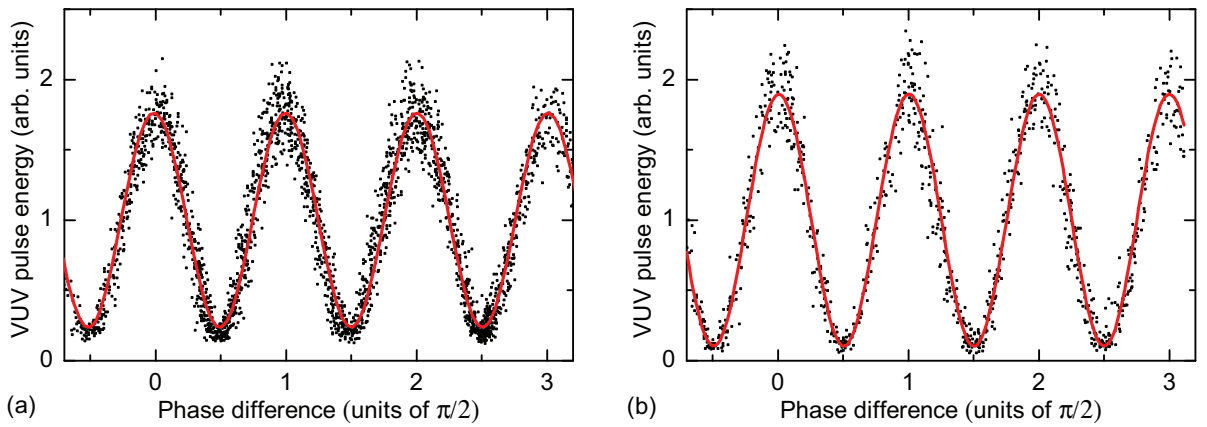

FIG. 3. (Color online) VUV intensity vs phase difference of the driving laser fields at fundamental laser wavelengths of (a) 512.0 nm (resonant) and (b) 512.7 nm. Black dots depict single-shot experimental data without any averaging. Laser intensities are $I_F = 1.4\ ^{\mathrm{TW}}/_{\mathrm{cm}^2}$ and $I_{SHG} = 6\ ^{\mathrm{GW}}/_{\mathrm{cm}^2}$. The red lines show fits with simple sine functions.

driven by the intense laser pulses towards longer wavelength. Spectroscopic investigations support this conclusion: The spectral lines broaden and strongly shift in the intensity regime of our experiment, i.e., a typical feature for excitations at large intensities.

Both data sets depicted in Fig. 3 show very strong quantum interference of the frequency conversion processes. This enables efficient control of the frequency conversion processes by proper choice of phase differences, e.g., pronounced suppression by destructive quantum interference or enhancement by constructive quantum interference. In our experiments, the difference between a large VUV signal at constructive and an almost vanishing VUV signal at destructive quantum interference reaches a factor of 18. To the best of our knowledge, there are only a few quantum interference experiments (for arbitrary systems or quantum processes) with similar modulation depths. In particular, there are no quantum interference experiments in frequency conversion of short laser pulses with such strong modulation depths, i.e., visibility up to 90%.

A. Variation of interference traces with laser intensities

We note that large visibility requires carefully matched conversion efficiencies on the two interfering frequency conversion pathways, i.e., fifth harmonic generation driven by the fundamental beam and four-wave mixing driven by the fundamental and the second harmonic beam. This is equivalent to matching equal light intensities for large contrast in a conventional light interferometer. As our two frequency conversion processes are highly nonlinear with different dependence upon the powers of the two driving lasers, proper matching is more difficult. Moreover, we must match the two pathways in the whole interaction volume. Fully perfect matching will be impossible, as in general the realistic spatial distribution of laser intensities varies in the focal volume parallel and perpendicular to the optical axis.

Perfect matching would work for perfect Gaussian beams with diameters $d_F/d_{SH} = \sqrt{2}$, which is very hard to achieve for high-power pulsed lasers. Thus the efficiency ratio of the two nonlinear frequency conversion processes of different order also spatially varies in the interaction volume. Nevertheless, as our above quantum interference data show, it is possible to come quite close to the limit of 100% visibility. We systematically investigate now the visibility of the quantum interference pattern with regard to the driving laser intensities. As only the ratio of the intensity matters, we keep the fundamental laser intensity fixed and monitor the variation of the visibility with the intensity of the second harmonic beam (see Fig. 4). We choose the fundamental wavelength close to the theoretical transition wavelength, i.e., neglecting Stark shifts. As the data in Fig. 4 show, for second harmonic intensities around 1.7 $^{\mathrm{GW}}/_{\mathrm{cm}^2}$, we reach a maximal visibility slightly below 80%, i.e., quite similar to the data in Fig. 3(a). Variations of the intensity by a factor of 2 reduce the visibility only by roughly 10%. Along with the experimental data, Fig. 4 also shows a simulation. For the simulation, we integrate Eq. (3) across the spatial laser beam profile. The integral is proportional to the relevant nonlinear polarization components and hence also the detected VUV pulse energies on the two interfering conversion pathways,

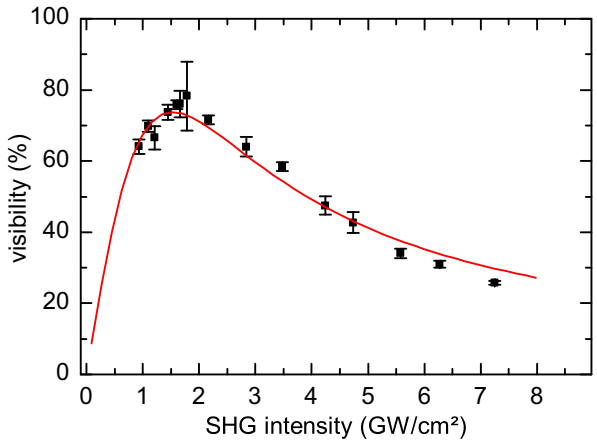

FIG. 4. (Color online) Visibility of quantum interference in VUV pulse energy at a fundamental wavelength of 512 nm with respect to phase variation plotted vs the relative ultraviolet intensity. Black squares show the mean visibility at a fundamental intensity of 0.9 $^{\mathrm{TW}}/_{\mathrm{cm}^2}$. The red line is a simplified calculation of the dependence.

i.e., $\propto \iint_{-\infty}^{-\infty} \mathrm{Re}\{I_{VUV}\}dxdy$. For the numerical integration we assume a transversal Gaussian intensity distribution in the laser foci and neglect variation of the intensity parallel to the optical axis, as the Rayleigh length of the foci is much longer than the width of the interaction region. Moreover, we neglect issues of phase matching. As the first one-photon transition occurs at a wavelength below 150 nm, the dispersion is shallow for both driving fields. In the simulation we allow for some residual misalignment of the laser foci in transversal direction. The calculation involves the ratio of unknown susceptibilities $\chi^{(3)}_{FWM}, \chi^{(5)}_{5HG}$, which remains as a free parameter to fit the simulation on the experimental data. As Fig. 4 shows, the simple model agrees very well with the experimental data. We obtain a fitted value of 23 μm for the transversal misalignment. From our measurements we estimate the spatial separation to be less than 15 μm, i.e., roughly in the same range as the fitted parameter. The calculated visibility then yields 87%. This is consistent with the red detuned measurement at a fundamental wavelength of 512.7 nm. This fact supports the assumption that dynamic stark shifts of the four-photon resonance reduce the maximum visibility for resonant excitation.

B. Variation of interference traces with the laser wavelength

The above measurement documented the important dependence of the visibility vs an experimental parameter, e.g., the laser intensities. In Fig. 3 we also saw changes of the visibility with the wavelength of the driving laser. Beyond the visibility, variation in the laser wavelengths also effects the phase difference between the laser pulses, and hence also changes the modulation period in the interference pattern. However, precise determination of modulation periods requires interference traces with many oscillations, i.e., many more oscillations than depicted in Fig. 3. This requires a very stable experimental setup to precisely vary and monitor the phase difference (i.e., the delay between the driving laser pulses) over a large range of many oscillation cycles. Our experimental setup with the reference HeNe laser in the

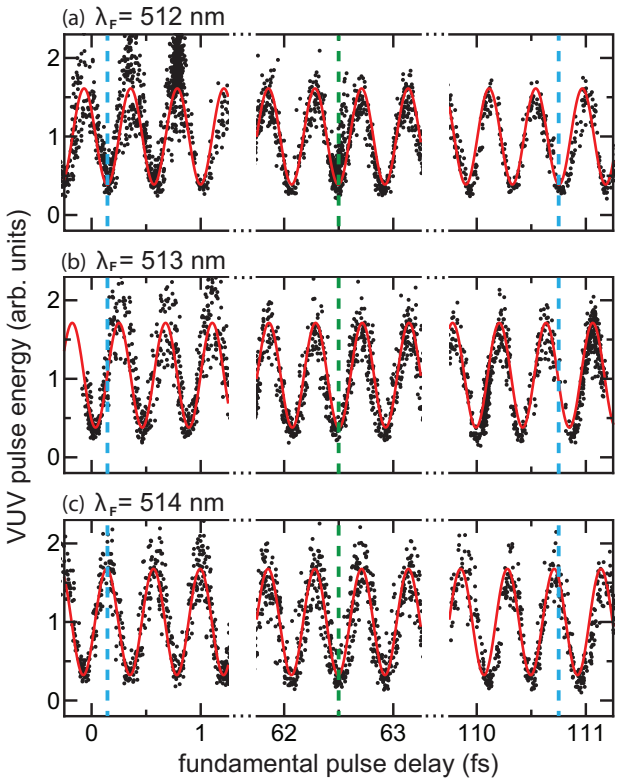

FIG. 5. (Color online) Long-range measurements of the VUV pulse energy vs phase difference of the driving laser fields at fundamental laser wavelengths of (a) 512 nm, (b) 513 nm, and (c) 514 nm. For better visibility, the plots show short sections of the recorded long interference traces only. Black dots depict single-shot experimental data without any averaging. Laser intensities are $I_F = 1.1\ ^{\mathrm{TW}}/_{\mathrm{cm}^2}$ and $I_{SHG} = 1.8\ ^{\mathrm{GW}}/_{\mathrm{cm}^2}$. Red lines show fits with simple sine functions. Dashed lines are to guide the eye (see text).

Mach-Zehnder-type delay line enables precise delays up to path length differences of 35 μm, corresponding to more than 110 fs, or more than 260 interference cycles. Figure 5 shows quantum interferences in our frequency conversion processes recorded over such a large oscillation interval with 260 oscillation cycles (for a fundamental wavelength of 514 nm) or 261 oscillation cycles (for a fundamental wavelength of 512 nm). As we want to compare the modulation periods of interference patterns at different fundamental wavelengths, in the x axes of Fig. 5 we give now pulse delays (rather than phase differences). For better readability we interrupted the x axes and show short selected sections of the long interference traces only (full large data sets not depicted here). During these long-range measurements (which also took a long time, i.e., 30 min for each short set of data), we took special care by control measurements that the setup for variation and determination of the phase differences remained very stable. As the interference traces in Fig. 5 show, the setup permits observation of pronounced quantum interferences also over the large number of oscillation cycles. We notice a slight decrease in signal pulse energy with increasing measurement time, caused by slight variations of experimental parameters, e.g., gas density. However, the visibility of the interference trace is not affected by the small signal loss and remains

TABLE I. Modulation period of the quantum interference signal for three driving wavelengths λ_F (in vacuum).

λ_F (nm)	Retrieved period (nm)	Expected period (nm)
512.00(15)	128.03(6)	128.00(4)
513.00(15)	128.27(7)	128.25(4)
514.00(15)	128.48(6)	128.50(4)

on a constant, high level. It is also clearly observed that the interference traces at different fundamental laser wavelengths steadily dephase, as expected due to their slightly different modulation period. While all traces are in phase for delays around 60 fs (as shown by the green dashed line), the trace at 514 nm fundamental wavelength collects a phase difference of π for delays of 0 and 110 fs (as shown by the blue dashed line).

Table I shows the modulation wavelength retrieved from the sine fits on the experimental data in Fig. 5. The errors in the retrieved modulation periods are due to the uncertainty $\Delta\lambda = 0.005$ nm in the wavelength of the HeNe reference laser, and a maximal statistical error of about 0.05 nm when retrieving the oscillation period from the quantum interference traces. Also, the expected oscillation period has an uncertainty of 0.04 nm due to limited accuracy in the determination of the fundamental laser wavelength. As expected, the modulation period grows with the fundamental wavelength divided by 4, i.e., it exactly follows the wavelength of the four-photon transition.

C. Simultaneous interference in population and frequency conversion

Our coupling scheme enables observation of quantum interferences also on a second detection channel. Excitation of atomic population to state $6p^2[5/2]_2$ is possible by two simultaneous pathways, i.e., (1) a four-photon excitation, driven by the fundamental radiation and (2) a two-photon excitation, driven by the second harmonic.

To probe the excited-state population, we collect the laser-induced fluorescence simultaneously to the frequency mixing

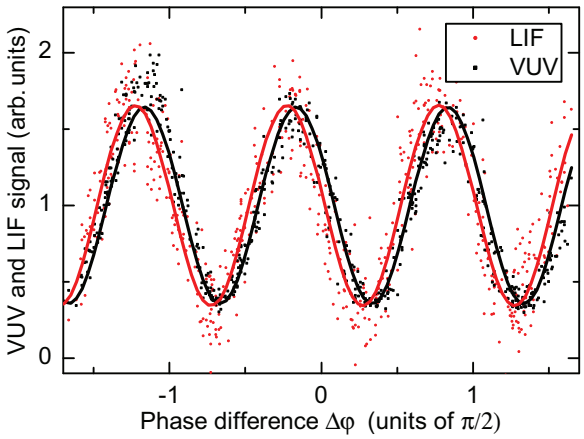

FIG. 6. (Color online) LIF (red circles) and VUV (black squares) intensities vs phase difference of the driving laser fields. The laser intensities are $I_F = 3.6\ ^{\mathrm{TW}}/_{\mathrm{cm}^2}$ and $I_{SHG} = 33\ ^{\mathrm{GW}}/_{\mathrm{cm}^2}$. Lines show fits with sine functions to the LIF signal (red line) and VUV signal (black line).

signal. We perform these measurements at rather high laser intensity in order to yield sufficiently large fluorescence signals for detection. The dependence of the frequency conversion and fluorescence signals vs the phase of the fundamental beam is shown in Fig. 6.

Strong quantum interferences are visible in both detection channels. As an interesting feature, we observe a small phase lag between the generated VUV pulse energy and population of the $6p^2[^5/_2]_2$ state. To confirm the finding, we repeated the measurement several times at resonant conditions (i.e., $\lambda_{fund} = 512.0$ nm). All data show the same phase lag of 0.03π at 512 nm fundamental wavelength, corresponding to a pulse delay of 7.8 nm. This phase lag can not be explained by some uncertainty of φ_F in our setup, since both signals are acquired simultaneously. Consequently, there is a phase lag of 0.12π with regard to the 128-nm oscillation period. Thus we suspect the phase lag in the quantum interferences to be due to the difference $\Delta_\chi - \Delta_\mu$ in atomic phase contributions [see Eqs. (5) and (4)].

V. CONCLUSION

We implemented and systematically studied quantum interferences in resonantly enhanced frequency up-conversion, driven by ultrashort (picosecond) laser pulses to generate vacuum-ultraviolet radiation. The quantum interferences are due to simultaneous resonantly enhanced four-wave mixing and fifth harmonic generation in a dense jet of xenon atoms. A four-photon transition is driven by intense laser pulses at visible wavelengths around 512 nm. The two-photon transition is driven by ultraviolet laser pulses around 256 nm. Another photon around 512 nm serves to drive fifth harmonic generation of the fundamental beam and simultaneous four-wave mixing with the ultraviolet radiation pulses, both yielding ultrashort radiation pulses at 102 nm. The two frequency conversion processes interfere, depending on the relative phase of the two driving laser beams. To precisely vary and monitor the relative phase, we implemented a Mach-Zehnder-type delay line, involving a reference laser to determine pulse delays with high accuracy. By appropriate choice of the phase, we get constructive interference (resulting in increased conversion efficiency) or destructive interference (resulting in reduced conversion efficiency). Proper matching of the laser intensities (and hence the excitation probabilities on the two interfering pathways) permits very pronounced constructive and destructive quantum interference with a visibility of 90%. This permits control of the frequency conversion by a factor of 18, as defined by the ratio of maximal and minimal frequency conversion yield. The stable and highly accurate phase control setup enables us to record strong quantum interferences for more than 260 oscillation cycles. We systematically study the dependence of the visibility upon the laser intensities and compare the experimental data with numerical simulations. The data show that large visibilities are possible in a broader intensity interval, allowing for variations by a factor of 2 in the intensities. Moreover, we investigate the variation of the modulation period in the interference patterns vs the wavelength of the driving fundamental laser pulses. In an extension of the experiment, simultaneously to frequency conversion we also monitor laser-induced fluorescence as a measure for the excitation probability to state $6p^2[^5/_2]_2$. Both the frequency conversion and fluorescence channel show similar quantum interferences with large modulation depth. However, a small phase lag of $\Delta\phi = 0.03\pi$ occurs between the interference traces of frequency conversion and fluorescence. We suspect the interesting feature to be due to an additional atomic phase acquired during frequency conversion by involvement of high-lying Rydberg states. The experiments exhibit a convincing demonstration of very pronounced quantum interferences also in the field of higher-order frequency conversion with ultrashort laser pulses, reaching a large modulation depth already very close to the theoretical limit.

ACKNOWLEDGMENTS

We acknowledge very valuable discussions with M. Shapiro (University of British Columbia, Vancouver) and financial support by the Deutsche Forschungsgemeinschaft (DFG).

[1] P. Brumer and M. Shapiro, Chem. Phys. Lett. **126**, 541 (1986).
[2] M. Shapiro and P. Brumer, *Quantum Control of Molecular Processes* (Wiley, New York, 2012).
[3] N. E. Karapanagioti, D. Xenakis, D. Charalambidis, and C. Fotakis, J. Phys. B **29**, 3599 (1996).
[4] D. Xenakis, N. E. Karapanagioti, C. Fotakis, and D. Charalambidis, Opt. Commun. **152**, 83 (1998).
[5] H. Muench, S. Chakrabarti, and T. Halfmann, Phys. Rev. A **82**, 033821 (2010).
[6] Y. Zhang, U. Khadka, B. Anderson, and M. Xiao, Phys. Rev. Lett. **102**, 013601 (2009).
[7] M. Aymar and M. Coulombe, At. Data Nucl. Data Tables **21**, 537 (1978).
[8] C. J. Humphreys and E. Paul, J. Opt. Soc. Am. **60**, 1302 (1970).
[9] E. Papastathopoulos, D. Xenakis, and D. Charalambidis, Phys. Rev. A **59**, 4840 (1999).
[10] T. Adachi, K. Kondo, and S. Watanabe, Appl. Phys. B **55**, 323 (1992).
[11] M. Gunawardena and D. S. Elliott, Phys. Rev. A **76**, 033412 (2007).